

This is a repository copy of *Structural and electronic determinants of lytic polysaccharide monooxygenase reactivity on polysaccharide substrates*.

White Rose Research Online URL for this paper:

<https://eprints.whiterose.ac.uk/123812/>

Version: Accepted Version

---

**Article:**

Simmons, Thomas J, Frandsen, Kristian E H, Ciano, Luisa [orcid.org/0000-0002-1667-0856](https://orcid.org/0000-0002-1667-0856) et al. (12 more authors) (2017) Structural and electronic determinants of lytic polysaccharide monooxygenase reactivity on polysaccharide substrates. *Nature Communications*. 1064 (2017). ISSN 2041-1723

<https://doi.org/10.1038/s41467-017-01247-3>

---

**Reuse**

This article is distributed under the terms of the Creative Commons Attribution (CC BY) licence. This licence allows you to distribute, remix, tweak, and build upon the work, even commercially, as long as you credit the authors for the original work. More information and the full terms of the licence here:

<https://creativecommons.org/licenses/>

**Takedown**

If you consider content in White Rose Research Online to be in breach of UK law, please notify us by emailing [eprints@whiterose.ac.uk](mailto:eprints@whiterose.ac.uk) including the URL of the record and the reason for the withdrawal request.

1 Structural and electronic determinants of lytic polysaccharide  
2 monooxygenase reactivity on polysaccharide substrates

3 Simmons TJ<sup>1\*</sup>, Frandsen KEH<sup>2\*</sup>, Ciano L<sup>3</sup>, Tryfona T<sup>1</sup>, Lenfant N<sup>4,5</sup>, Poulsen JC<sup>2</sup>, Wilson  
4 LFL<sup>1</sup>, Tandrup T<sup>2</sup>, Tovborg M<sup>6</sup>, Schnorr K<sup>6</sup>, Johansen KS<sup>7</sup>, Henrissat B<sup>4,5,8</sup>, Walton PH<sup>3</sup>, Lo  
5 Leggio L<sup>2</sup> & Dupree P<sup>1</sup>.

6 1. Department of Biochemistry, University of Cambridge, Cambridge, UK.

7 2. Department of Chemistry, University of Copenhagen, Copenhagen, Denmark.

8 3. Department of Chemistry, University of York, York, UK.

9 4. Architecture et Fonction des Macromolécules Biologiques (AFMB), CNRS, Aix-Marseille  
10 Université, Marseille, France.

11 5. Institut National de la Recherche Agronomique (INRA), AFMB, Marseille, France.

12 6. Novozymes A/S, Bagsvaerd, Denmark.

13 7. Department of Geoscience and Natural Resources Management, Copenhagen University,  
14 Frederiksberg, Denmark

15 8. Department of Biological Sciences, King Abdulaziz University, Jeddah, Saudi Arabia.

16 \*These authors contributed equally to this work

17 Correspondence and requests for material should be sent to L.L.L. (email: leila@chem.ku.dk) or

18 P.D. (email: pd101@cam.ac.uk)

## Abstract

Lytic polysaccharide monooxygenases (LPMOs) are industrially important copper-dependent enzymes that oxidatively cleave polysaccharides. We studied two closely related AA9-family LPMOs from *Lentinus similis* (LsAA9A) and *Collariella virescens* (CvAA9A). LsAA9A and CvAA9A cleave a range of polysaccharides, including cellulose, xyloglucan, mixed-linkage glucan, and glucomannan. LsAA9A additionally cleaves isolated xylan substrates, the first LPMO to show such activity. Insights into the determinants of specificity come from the structures of CvAA9A and of LsAA9A bound to cellulosic and non-cellulosic oligosaccharides. EPR spectra further reveal differences in copper coordination on binding of xylan compared to glucans. LsAA9A activity is notably less sensitive to reducing agent potential on xylan when compared to other substrates, suggesting a different mechanistic pathway for the cleavage of xylan. These data show that AA9 LPMOs can display different apparent substrate specificities dependent upon both productive protein:carbohydrate interactions across a binding surface and also electronic considerations at the copper active site.

The need for sustainable sources of energy and materials has spurred significant research efforts toward a greater understanding of the biological catabolism of lignocellulose, the world's most abundant source of renewable material and bioenergy<sup>1,2</sup>. The inherent recalcitrance of lignocellulose, however, is one of the major barriers to the utilization of biomass. This recalcitrance is a consequence of both the heterogeneous composition and the often semi-crystalline association of the polymers<sup>3,4</sup>. In addressing the problem of recalcitrance, multiple potential means have been proposed and assessed, including chemical, mechanical and enzymatic methods. Advances in enzyme cocktail formulations that accelerate the saccharification step of cell wall breakdown<sup>5</sup>, in particular the inclusion of the lytic polysaccharide mono-oxygenases (LPMOs)<sup>6</sup>, are helping cellulosic-ethanol biorefineries move toward both commercial and environmental viability.

LPMOs are O<sub>2</sub> and reducing-agent dependent copper metalloenzymes now classified as Auxiliary Activity families AA9–AA11 and AA13<sup>7-11</sup>. Extensive spectroscopic and structural studies on LPMOs have shown that the enzyme's active site contains a single copper ion, which is coordinated by the amino terminus nitrogen atom, by a side chain nitrogen atom of the N-terminal histidine, and by the side chain nitrogen atom of an additional histidine, in a structural motif known as the histidine brace<sup>12</sup>. What is distinctive about LPMOs is that they oxidatively rather than hydrolytically cleave polysaccharides producing saccharides with oxidized ends<sup>13</sup>. LPMOs augment the action of other polysaccharide-degrading enzymes, and accordingly much research attention is devoted to a greater understanding of the enzymatic mechanism and the range of LPMO saccharide substrates.

It was first shown that LPMOs could boost the action of cellulases on cellulose and chitin<sup>14-16</sup>, but LPMOs are now known to act on several crystalline substrates such as chitin, cellulose and retrograded starch<sup>10-12,17</sup>. Later, enzymes with activity against non-crystalline and oligomeric structures were identified<sup>18,19</sup>. Furthermore, fungal AA9 LPMOs have been shown to be active on soluble substrates such as xyloglucan, mixed-linkage glucan and glucomannan<sup>19-22</sup> and on cellulose-bound xylan<sup>23</sup>. Conspicuously, an LPMO active on isolated xylan has not been reported. This range of reported substrates however will likely grow. The large number and sequence diversity of LPMOs that individual fungi maintain<sup>24</sup>,

and their disparate expression profiles when the fungi are grown on different polysaccharide substrates<sup>25,26</sup>, signal that AA9 LPMOs do have distinct, and functionally significant, polysaccharide substrate specificities, although some evolutionary diversity of LPMOs likely arises through their use of different reducing systems<sup>27,28</sup>.

The root causes of LPMO substrate specificity remain poorly understood. This is because LPMO chemistry is a subtle and complex combination of structural and electronic factors, both of which must be taken into account when developing an understanding of the mechanism of action<sup>29</sup>. The structure-function relationship of substrate specificity and regiospecificity has been recently reviewed<sup>30,31</sup>. Insight into LPMO:substrate binding can be gained from the structures of LPMOs<sup>30</sup> and combined structural and spectroscopic studies of LPMOs in contact with substrate. Recent ITC, NMR and docking studies of an AA9 LPMO from *Neurospora crassa* in contact with oligosaccharides revealed that more extended substrates had significantly higher binding affinities. This is in accord with a multi-point interaction of the substrate with the LPMO surface where the surface loops in some LPMOs remote from the active site enhance binding affinity<sup>21</sup>. The study also showed that a single Cell<sub>6</sub> chain likely spans the copper active site from the -3 to +3 or -2 to +4 subsites (subdivisions of the binding cleft numbered relative to the site of cleavage<sup>32</sup>), in which the L3 loop (important for interactions with the +3/+4 subsites) and the LC loop (important for binding to approximately -4 subsite) lie at somewhat extended distances from the copper active site. Detailed insight into an AA9 LPMO-substrate interaction came from the first crystal structures of LPMO:oligosaccharide complexes: *Lentinus similis* AA9A (LsAA9A) bound to cellohexaose (Cell<sub>6</sub>) and Cell<sub>3</sub><sup>33</sup>. Cell<sub>6</sub> was shown to bind at subsites -4 to +2 via interactions with aromatic residues, the N-terminal His and a conserved Tyr as well as a number of hydrogen-bonds with other residues in a contoured binding surface on the LPMO. The +2 glucosyl residue exhibits a set of well-defined hydrogen-bonding interactions with amino-acid side chains (Asn28, His66 and Asn67) essentially locking this residue into a fixed position with respect to the active site.

Electronic factors around the active site also play a key role in determining reactive mechanism. Changes in the electronic structure of the copper ion, an important factor in the ability of the copper ion to activate O<sub>2</sub>, occur upon substrate binding to LsAA9A<sup>33</sup>. Furthermore, in an illustration of the complexity of substrate-LPMO interaction and the

subtle interplay of electronic and structural factors, Cell<sub>6</sub> is bound synergistically with an exogenous ligand on the copper ion. It is likely that the oxidative mechanism adopted by LPMOs can proceed via one or more of several different routes<sup>34</sup>, the determinants of which depend to varying extents on the substrate, the reducing agent reducing potential and the positioning of the substrate on the LPMO surface. For instance, the means by which electrons are donated to the LPMO active site modulate the apparent range of reactivity<sup>28,35</sup>.

The detailed molecular and electronic insights of the LPMO-substrate interaction afforded by *combined* biochemical, X-ray diffraction and EPR spectroscopic studies can significantly enhance our understanding of LPMO reactivity. We report herein a study into the principal structural and electronic factors of the reactivity of two AA9 LPMOs with a range of substrates. Through X-ray crystal structures studies of LsAA9A with bound substrates we illustrate how binding cleft interactions dictate the site of polysaccharide attack. Through comparison with the CvAA9A structure, also determined here, we suggest some structural determinants of specificity for the two enzymes. LsAA9A is active on isolated xylan, but this activity is associated with a distinct low sensitivity to reducing agent potential and a different copper co-ordination at the active site, which together reveal an alternative mechanistic pathway for LPMO action on this substrate. These data show how AA9 LPMO substrate cleavage is dependent upon both productive protein:carbohydrate interactions across a binding surface and also electronic considerations at the active site.

## Results

### CvAA9A is an additional AA9 LPMO active on cello-oligosaccharides

To help understand the basis of AA9 substrate specificity, we searched for enzymes related to LsAA9A which might also cleave soluble oligosaccharides. Because LPMOs exhibit high variability in their C-termini, we performed a large-scale alignment of LPMO protein sequences using their N-terminal portion<sup>36</sup>. We selected 98 AA9 sequences that were highly similar in their N-terminal half to LsAA9A and 326 sequences that were highly similar to TaAA9A in the same region. TaAA9A was used for comparison purposes, since it does not show the ability to cleave soluble oligosaccharides. After adding the sequences

of 20 AA9 enzymes studied in the literature, a distance tree was built with the resulting 444 AA9 sequences (Fig. 1a, Supplementary Table 1). The tree clearly places *LsAA9A* and *TaAA9A* in distinct clades. From the *LsAA9A* clade, we identified an LPMO from *Collariella virescens* (*CvAA9A*; 46% sequence similarity to *LsAA9A*) that lacks some residues observed by Frandsen et al.<sup>33</sup> as being involved in enzyme-substrate interactions (Supplementary Fig. 1). All three of the subsite +2 substrate-binding residues in *LsAA9A* (Asn28, His66 and Asn67) are different in *CvAA9A* (Thr28, Arg67 and Val68) (Supplementary Fig. 1). To study the activity of *CvAA9A*, the enzyme was expressed in *Aspergillus oryzae* and successfully purified from the fermentation broth. (Note that expression in this fungal host preserves the natural side-chain methylation at the N-terminal histidine, in contrast to fungal LPMO expression in *Pichia pastoris* and bacterial systems.) On phosphoric acid-swollen cellulose (PASC), *CvAA9A* produced a range of cello-oligosaccharides (Fig. 1b). The cello-oligosaccharide product profile of *CvAA9A* was similar to that of *LsAA9A* and notably shorter than those produced by *TaAA9A*. Indeed, *CvAA9A* readily degraded Cell<sub>6</sub>-2-aminobenzamide (Cell<sub>6</sub>-2AB) using a C4-oxidising mechanism to yield Cell<sub>3</sub> and oxidized Cell<sub>3</sub>-2AB (Supplementary Fig. 2), like *LsAA9A* but unlike *TaAA9A*<sup>33</sup>. Therefore, the distance relationships between the three enzymes, as measured using the N-terminal comparison method above, mirror the similarities in activities of the enzymes.

### Position-specific cleavage of a range of hemicelluloses

We next determined whether the *LsAA9A* and *CvAA9A* enzymes are active on a range of  $\beta$ -(1 $\rightarrow$ 4)-D-glucan-related polysaccharides (Fig. 2, Table 1). Mixed-linkage glucan (MLG) is a  $\beta$ -D-glucan in which three to four (1 $\rightarrow$ 4)-linked residues (Cell<sub>3</sub>, Cell<sub>4</sub>) are separated by single (1 $\rightarrow$ 3) bonds, glucomannan has a backbone randomly composed of  $\beta$ -(1 $\rightarrow$ 4)-D-glucosyl and  $\beta$ -(1 $\rightarrow$ 4)-D-mannosyl residues, xyloglucan is a  $\beta$ -(1 $\rightarrow$ 4)-D-glucan with  $\alpha$ -(1 $\rightarrow$ 6)-D-xylosyl branches, and xylan is a polymer of  $\beta$ -(1 $\rightarrow$ 4)-D-xylosyl residues that is similar to  $\beta$ -(1 $\rightarrow$ 4)-D-glucan but lacks C6 groups (Fig. 2b). Both *LsAA9A* and *CvAA9A* showed activity against MLG, glucomannan and xyloglucan, producing a range of oligosaccharide products (Fig. 2a). *LsAA9A* also showed some activity on xylan whereas *CvAA9A* showed no measurable activity on this substrate. No LPMO activity was observed on starch ( $\alpha$ -(1 $\rightarrow$ 4)-D-glucan), laminarin ( $\beta$ -(1 $\rightarrow$ 3)-D-glucan) or chitin (poly  $\beta$ -(1 $\rightarrow$ 4)-D-

GlcNAc) (Supplementary Fig. 3). Altogether, these activities indicate that both *LsAA9A* and *CvAA9A* enzymes only cleave near  $\beta$ -(1 $\rightarrow$ 4)-bonds, and that some variation to the cellulosic  $\beta$ -(1 $\rightarrow$ 4)-D-glucan, including substitution, linkage and backbone residue, can be accommodated at or near the site of cleavage by both of the enzymes.

To identify precise substrate cleavage sites, we studied the products of both *LsAA9A* and *CvAA9A* cleavage of MLG, glucomannan, xyloglucan and xylan (in the case of *LsAA9A*) polysaccharides by MALDI-ToF MS. Minor double oxidation products were observed, indicating cleavage of these hemicelluloses and PASC using both C1- and C4-oxidising mechanisms (Fig. 3; Supplementary Fig. 4, Table 1). We further investigated the site of attack on these different hemicelluloses using differing protocols. On MLG, we observed in the MALDI data a predominance of DP 4, 7 and 10 oligosaccharides indicating that each enzyme favors cleaving within Cell<sub>4</sub> regions over Cell<sub>3</sub> regions (Fig. 3). The inability of *LsAA9A* and *CvAA9A* to cleave  $\beta$ -Glc-(1 $\rightarrow$ 4)- $\beta$ -Glc-(1 $\rightarrow$ 3)- $\beta$ -Glc-(1 $\rightarrow$ 4)-Glc (G4G3G4G), despite their ability to cleave Cell<sub>4</sub> (G4G4G4G) (Supplementary Fig. 5), supports the hypothesis that neither enzyme can cleave at  $\beta$ -(1 $\rightarrow$ 3)-bonds and require substantial  $\beta$ -(1 $\rightarrow$ 4)-linked regions for cleavage. On glucomannan, we employed High-Performance Anion-Exchange Chromatography (HPAEC) analysis of trifluoroacetic acid (TFA) hydrolysates of digestion products to assess the site of cleavage. Notably, the data indicated that cleavage can occur not only between glucosyl residues, but also with mannose at the +1 or -1 subsite (Supplementary Fig. 6). In order to deduce site of attack on xyloglucan we employed xyloglucan DP14–18 oligosaccharides (Supplementary Fig. 7). Inspection of the position of substituted glucose (Glc) in the products indicated that xylosyl substitution of Glc at O-6 was accommodated at the -3, -2, -1, +2 and +3 subsites but unsubstituted Glc was always required at subsite +1. In contrast to the *LsAA9A* and *CvAA9A* products on polysaccharides, *LsAA9A* degraded Xyl<sub>6</sub>-2AB to yield two trimers using solely a C4-oxidising mechanism (Supplementary Fig. 8), analogous to cleavage of Cell<sub>6</sub>-2AB by both *LsAA9A*<sup>33</sup> and *CvAA9A* (Supplementary Fig. 2).

To allow a semi-quantitative determination of the influence of sugar structures on enzyme activity, we probed *LsAA9A* and *CvAA9A* cleavage of the soluble Cell<sub>6</sub>, xylohexaose (Xyl<sub>6</sub>) and mannohexaose (Man<sub>6</sub>) oligosaccharides (Supplementary Fig. 9). The *LsAA9A* activity against Cell<sub>6</sub> was substantially (~100-fold) better than its activity on Xyl<sub>6</sub>. Consistent with



the absence of activity on glucuronoxylan, CvAA9A activity on Xyl<sub>6</sub> was almost undetectable (~1,000-fold less than Cell<sub>6</sub> activity). Although both enzymes showed activity on glucomannan and can cleave adjacent to mannose, activity was scarcely detectable on Man<sub>6</sub> (~10,000-fold less than Cell<sub>6</sub>), indicating that the enzymes require some Glc residues within a mannan backbone for activity.

Recent results show dependence of the LPMO action on reductant strength<sup>28,37</sup>. We found that cleavages of MLG, glucomannan and xyloglucan by LsAA9A were sensitive to reducing agent potential, with ascorbate as reductant yielding much higher amount of product (Fig. 4a). In contrast, cleavage of xylan was not sensitive. We corroborated this finding with oligosaccharides, observing that Xyl<sub>6</sub> was poorly sensitive to reducing agent potential, unlike cleavage of Cell<sub>6</sub> where LsAA9A showed much greater activity with ascorbate than pyrogallol<sup>33</sup> (Fig. 4b).

### **LsAA9A: and CvAA9A:cello-oligosaccharide structures**

To help understand the structural basis of LPMO attack on different substrates, we employed crystallographic analyses. We report here an LsAA9A:Cell<sub>5</sub> complex (Fig. 5 and Supplementary Table 4 and 5) which, owing to a lack of significant substrate contacts to symmetry-related molecules, is a more faithful depiction of the binding conformation of a single oligosaccharide to LsAA9A as compared to the original LsAA9A:Cell<sub>6</sub> structure described by Frandsen et al<sup>33</sup>. Tyr203 stacking is still a major interaction in LsAA9A:Cell<sub>5</sub> but a new hydrogen bond is seen between O6 and Asp150 at subsite -3, and glycosidic torsion angles are closer to ideal values (Supplementary Table 2). Other interacting residues at the negative subsites are Glu148, Arg159 and Ser77 (Fig. 5; Supplementary Table 3). Like the LsAA9A:Cell<sub>6</sub> structure<sup>33</sup>, the main interactions to Cell<sub>5</sub> are a network of hydrogen bonds by Asn28, His66 and Asn67 interacting with O2 and O3 at subsite +2, and the interaction with MeHis1 at subsite +1<sup>38</sup>.

To understand better how protein structure might influence the similarities and differences in CvAA9A and LsAA9A substrate cleavage patterns, the X-ray crystal structure of CvAA9A was solved (Supplementary Fig. 10 and Supplementary Tables 3-5). The Cu-coordinating amino acid residues are MeHis1 and His79 (with equatorial distances to the

Cu ranging from 2.0-2.1Å), while a non-coordinating Tyr169 occupies the axial position (2.6-2.8Å). No exogenous ligands are evident within 3.0 Å of the Cu ion indicating that the active site is mostly in a photoreduced Cu(I) state. A “pocket-water” is bound in an H-bond network with the amide-nitrogen and oxygen of Asp76 and MeHis1, respectively. The active site geometry of CvAA9A thus closely resembles that of LsAA9A (Supplementary Fig. 10c). However, there are some amino acid differences in CvAA9A compared to LsAA9A at subsites +2 and -1. Crystals of CvAA9A were soaked with Cell<sub>3</sub> and Cell<sub>6</sub> oligosaccharides but this did not result in any catalytically relevant complex.

### **LsAA9A:hemicellulose oligosaccharide structures**

To study the structural determinants of the LsAA9A positional specificity of cleavage, a number of LsAA9A crystal structures in complex with MLG, glucomannan and xylo-oligosaccharides were solved (see Supplementary Tables 2–5 for experimental and crystallographic data and refinement information, hydrogen bonding interactions between enzyme and ligand, and ligand conformations). Soaking experiments with commercially available xyloglucan fragments failed to produce crystallographic complexes, possibly because the substrate oligosaccharides are large and binding likely to be impeded by crystal contacts.

#### *Complexes with MLG tetrasaccharide*

LsAA9A crystals were soaked with two different MLG tetrasaccharides, each with a single β-(1→3)-linkage: G4G4G3G and G4G3G4G. Interestingly, the LsAA9A:G4G4G3G complex did not reveal any β-(1→3)-linkages. An apparent Cell<sub>4</sub> substrate appears to be bound from subsite -2 to +2 (Supplementary Fig. 11) giving essentially identical interactions as the -2 to +2 glucosyl residues in the LsAA9A:Cell<sub>5</sub> complex. We interpret this result as the β-(1→4)-glucan (Cell<sub>3</sub>) part of the substrate being bound in two overlapping conformations in different asymmetric units from subsites -2 to +1 and -1 to +2, while the β-(1→3)-glucosidic residues are completely disordered in both cases. A structure of LsAA9A crystals soaked with G4G3G4G (not shown) showed very little difference density, which could not be convincingly modelled, further indicating that the

enzyme needs at least two consecutive  $\beta$ -(1 $\rightarrow$ 4)-linkages (a Cell<sub>3</sub> unit) for recognition and efficient binding.

#### *Complexes with glucomannan oligosaccharides*

LsAA9A crystals were soaked with a mixture of glucomannan oligosaccharides. The resulting difference density was well defined clearly showing glycosyl units occupying subsites -3 to +2, additional density at -4 and some residual density occupying subsite +3 (Fig. 6a and 6c). Consistent with the activity data, the structure unequivocally showed a mannosyl unit at the +1 subsite, while glucosyl units were clearly observable at -2, -1 and +2 subsites. Moreover the C2 hydroxyl of the mannosyl unit at subsite +1 points towards the face of the imidazole side chain of MeHis1, and the axial water molecule is displaced (Fig. 6b and 6d). The identity of the glycosyl unit at subsite -3 is ambiguous though best modelled as mannose. The density of the glycosyl unit at subsite -4 is weak and occupies a very similar position as the corresponding unit in the LsAA9A:Cell<sub>6</sub> complex, as does the glycosyl unit at subsite -3, due to similar crystal constraints.

#### *Complexes with xylo-oligosaccharide*

Whereas in crystals soaked with Xyl<sub>3</sub> and Xyl<sub>4</sub> (Supplementary Tables 2–5) the oligosaccharides did not fully span the active site, LsAA9A:Xyl<sub>5</sub> crystals revealed very well-defined density from subsites -3 to +2 (Fig. 7a). The oligosaccharide position at subsites -3 to -1 are similar to LsAA9A:Cell<sub>5</sub>, but with a translation of about half a pyranose unit in the non-reducing end direction. In contrast, the plane of the xyloside unit at subsite +1 is rotated approximately 90° compared to the corresponding glucosidic unit, while the xyloside residue binding +2 is rotated approximately 180° (Fig. 7d, Supplementary Table 2). As a result xylose at subsite +1 does not stack with MeHis1, and in fact appears to have no interactions with the enzyme, while the same residues that bind the subsite +2 glucosyl residue in the LsAA9A:Cell<sub>5</sub> structure, Asn28, His66 and Asn67, interact here with O1, O5 and O1 of the +2 xyloside residue, respectively (Fig. 7c Supplementary Table 3). A structure of LsAA9A:Xyl<sub>5</sub> determined from a low X-ray dose data collection showed the substrate bound similarly, and revealed a mix of water/Cl<sup>-</sup> in the axial position and a fully occupied equatorial water on the active site copper (Fig. 7b). Thus, in contrast to binding

of cello- or glucomannan oligosaccharides, the axial water was not displaced by binding of Xyl<sub>5</sub>.

## **EPR data suggest alternative LsAA9A substrate binding modes**

We studied substrate binding on both LsAA9A and CvAA9A using electron paramagnetic resonance (EPR) spectroscopy (Table 2) to investigate the electronic state of the active site copper upon binding. As has been shown by Frandsen et al.<sup>33</sup> and Courtade et al.<sup>21</sup>, the binding affinity of oligosaccharide substrates is significantly affected by the presence of the exogenous ligand on the copper ion. Accordingly, EPR experiments were carried out in both the absence and presence of 200 mM chloride (1.0 M chloride for Xyl<sub>6</sub> studies). Furthermore, experiments were carried out at high substrate concentration to maximize substrate binding. For LsAA9A a wide range of substrates was tested. In all cases, the parallel region of the spectra could be modelled with reliable  $g_z$  and  $|A_z|$  values, giving some insight into the electronic nature of the copper ion. Perpendicular values were less reliable due to the second-order nature of the spectra in this region, and are therefore not used in the analysis, although the appearance of superhyperfine coupling to ligands in this region was apparent in some cases (Table 2, Supplementary Fig. 12) and used as an indication of increased metal-ligand covalency in the singly-occupied molecular orbital (SOMO), as previously discussed by Frandsen et al.<sup>33</sup>. In all cases apart from xylan, the addition of substrate gave perturbation of the Cu spin Hamiltonian parameters similar to that already reported by Frandsen et al.<sup>33</sup> In particular, shifts in  $g_z$  values to ca 2.23 (along with the appearance of strong superhyperfine coupling) were seen upon addition of Avicel, glucomannan and xyloglucan, indicative of chloride coordination to the copper ion in the equatorial position of the copper coordination sphere. These shifts are analogous to those of LsAA9A interacting with Cell<sub>6</sub> and PASC<sup>33</sup>. In contrast, addition of Xyl<sub>6</sub> did not give significant shifts in  $g_z$  but did give perturbations in the  $|A_z|$  value, with the appearance of superhyperfine coupling indicative of a second species different from that formed with Cell<sub>6</sub>. The EPR spectra of LsAA9A binding to Xyl<sub>6</sub> and xylan are indicative of substrate binding to the enzyme (although binding of Xyl<sub>6</sub> could be achieved only at high chloride concentrations), but without the chloride occupying the equatorial coordination position on the copper ion, revealing that these substrates drive an electronic state at the copper ion that is different to that of the other substrates. EPR perturbation was seen upon addition of

Cell<sub>6</sub> to CvAA9A but not with Xyl<sub>6</sub>, consistent with the observed activity on Cell<sub>6</sub> and not Xyl<sub>6</sub> (Fig.8 and Supplementary Fig.13).

## Discussion

Our understanding of the molecular basis for substrate binding and cleavage has been aided by the recent report of a crystal structure of LsAA9A in complex with Cell<sub>3</sub> and Cell<sub>6</sub>, as well as biochemical and EPR data for LsAA9A on cellulosic substrates<sup>33</sup>. Here, we have extended this biochemical, EPR and structural analysis by using a range of substrates as well as an additional related enzyme, CvAA9A, to provide a better insight into substrate specificity.

Extensive probing of LsAA9A and CvAA9A substrate specificity showed that both cleave a range of cellulosic and non-cellulosic substrates, some of which have been shown for other AA9s<sup>19,20,22,23,27,29,35,39-41</sup>. We made a number of novel observations. Notably, LsAA9A activity on xylan and xylo-oligosaccharides is the first report of LPMO cleavage of isolated xylan; this may have important implications for the use of LPMOs in biotechnological contexts. LPMO activity on xylan has been observed before for M<sub>1</sub>LPMO9A<sup>23</sup>, but only on xylan associated with cellulose. We also observe that both LsAA9A and CvAA9A are able to cleave glycosidic bonds adjacent to mannosyl residues (Supplementary Fig. 6), which occur interspersed randomly with glucosyl residues in glucomannan, a biochemical observation supported by the LsAA9A:glucomannan oligosaccharide structure, which unambiguously shows a mannosyl residue at subsite +1. We also noticed substrate-specific oxidation profiles, namely that LsAA9A and CvAA9A cleaved small oligosaccharides using a C4-oxidising mechanism whereas they cleaved polysaccharides with both C1- and C4-oxidising mechanisms in varying proportions. Assuming a copper-based oxidative species, the similar distances between both C1 and C4 axial protons and the active oxygen species, as noted in Frandsen et al.<sup>33</sup>, may allow slight differences in substrate binding to switch the C-H bond that is closest to attack. Substrate binding differences may also subtly alter the electronics at the copper site, which potentially could also favour a specific oxidation site. Oxidation regioselectivity is therefore

less likely to be a strong functional constraint. This is in agreement with the presence of C1 and C4 regiospecificity in several clades in the N-terminal sequence similarity tree (Fig. 1). On the other hand, the tree enabled us successfully to predict that *LsAA9A* and *CvAA9A* might have similarities in having activity on a range of soluble substrates.

Our investigation highlighted many examples of the way in which substrate specificity and the site of attack on a polysaccharide is dictated by binding cleft interactions with the substrate. For example, *LsAA9A*'s preference to cleave Cell<sub>4</sub> into Cell<sub>2</sub> (as shown for *NdLPMO9C*<sup>18</sup>), compared to the product profile of *CvAA9A* of Cell<sub>3</sub>, Cell<sub>2</sub> and Glc (Supplementary Fig. 5), could be attributed to binding cleft interactions at the +2 subsite. This is because though *CvAA9A* shares the same fold, active site co-ordination and overall structure with *LsAA9A*, it lacks all three of the subsite +2 substrate-binding residues in *LsAA9A* (Asn28, His66 and Asn67) (Fig. 5; Supplementary Fig. 1). This suggests that, while *LsAA9A* binds Cell<sub>4</sub> from subsite -2 to +2, *CvAA9A* binds between subsites -3 and +1.

The structural data provide a molecular rationale for how *LsAA9A* is able to catalyse the unexpected cleavage of mannose-containing bonds. The *LsAA9A*:glucomannan oligosaccharide crystal structure shows the presence of a mannose (the C2 epimer of Glc), and essentially no Glc, at subsite +1. Talose (C4 epimer of mannose) and galactose (C4 epimer of Glc) arose from the reduction of C4-oxidised cleavage products (Supplementary Fig. 6), also suggesting both mannosyl and glucosyl occupation of subsite +1. We have previously described that the glucosyl unit at the +1 subsite in *LsAA9A* Cell<sub>3</sub> and Cell<sub>6</sub> complexes<sup>33,38</sup> interacts with MeHis1 through its  $\beta$ -face, and while glucose can make carbohydrate-aromatic stacking interactions<sup>42</sup> through both faces of the pyranose ring,  $\beta$ -mannose is believed to have absolute preference for interactions through its  $\alpha$ -face due to its axial C2-hydroxyl. Nonetheless, determination of the crystal structure of glucomannan fragments with *LsAA9A* confirmed that this type of interaction takes place, and the mannosyl residue at the +1 subsites interacts with MeHis through its  $\beta$ -face with an O5-imidazole ring centre distance of 3.6 Å (Fig 6d) (compared to 3.4-3.5 Å for the cello-oligosaccharide complexes). No similar interactions could be found through a search in the PDB. We did not observe a mannosyl residue at the -1 subsite in the structure, but it

would cause no steric clash and so could be readily accommodated (though it would cause the loss of a hydrogen bond interaction with Ser77).

Although we were unable to obtain a structure with xyloglucan oligosaccharides bound, our observation that both *LsAA9A* and *CvAA9A* cleaved xyloglucan DP14–18 oligomers with the sole unsubstituted backbone glucosyl residues at subsite +1 (XXX/GXXXGol; as found for *NdLPMO9C*<sup>19</sup>) is consistent with the binding of xyloglucan's celulosyl backbone being similar to the binding of cello-oligosaccharides. This would suggest that the *LsAA9A* could tolerate glucosyl residues with C6 xylosyl substitutions at subsites –1 or +2, but not at +1 where the C6 hydroxymethyl group occludes the copper axial binding site, and displaces the axial water.

*LsAA9A* under the selected conditions degraded Xyl<sub>6</sub> with about 1/100 the efficiency as Cell<sub>6</sub>, while *CvAA9A* left Xyl<sub>6</sub> essentially untouched at all conditions tested (Supplementary Fig. 9). The differences in key amino acids involved in defining the *LsAA9A* and *CvAA9A* subsites, particularly the +2 subsite (vide supra) (Supplementary Fig. 1; Fig. 5), are likely an important factor in *LsAA9A*'s superior xylan-degrading activity.

Our observation in *LsAA9A* complexes that MLG oligosaccharides were unable to bind with  $\beta$ -(1→3)-glucan bonds near the active site are consistent with our observation that both *LsAA9A* and *CvAA9A* favour the cleavage of celulosyl regions in MLG.

Not all aspects of substrate specificity could be explained through binding cleft interactions. Rather, aspects of the specificity differences appear to be mechanistic in origin and relate to the reactivity of different substrates. The high activity, spectroscopy data and structures of *LsAA9A* and *CvAA9A* with  $\beta$ -(1→4)-glucan substrates leads us to suggest the effective oxidative mechanism deployed in these situations may be regarded as a 'canonical pathway'. It is clear, however, that LPMOs may also have other 'non-canonical pathway' mechanisms, as exemplified by the differences between binding, spectroscopy and structures of *LsAA9A* with Xyl<sub>6</sub>. The crystallographic and EPR data show that a chloride ion – an oxygen species mimic – is not recruited into the copper's equatorial binding site upon xylooligosaccharide substrate binding, as happens in the canonical mechanism described by Frandsen et al<sup>33</sup>. The aldopentose nature of xylose categorically excludes the synergistic binding of saccharide ligand and molecular oxygen which is

brought about by a bridging “pocket” water molecule between the C6-hydroxymethyl group of Glc and the amino terminus of the enzyme. This suggests a different oxidative mechanism may well be in operation for the cleavage of xylose-based substrates by *LsAA9A*. Indeed, as has already been proposed by Kjaergaard et al<sup>43</sup>, activation of O<sub>2</sub> by an AA9 from *Thermoascus aurantiacus* probably gives formation of a copper-bound superoxide or hydrosuperoxide (HO<sub>2</sub>) through associative displacement of a superoxide anion by a water molecule through the axial coordination site on the copper ion. In particular, a superoxide ion bound to the copper in the axial position would be in position to cleave a saccharidic chain by direct attack. Such a mechanism is expected when the axial water molecule on the copper ion is *not* displaced by the binding of substrate, as is the case with the binding of Xyl<sub>5</sub> to *LsAA9A*. From the low dose *LsAA9A*:Xyl<sub>5</sub> structure described herein, the axial ligand is clearly present on the copper ion, though it is best modelled as a mixture of chloride and water, and the Tyr-O distance (2.86 Å) is not shortened compared to the un-complexed low dose structure (2.72Å - PDB 5ACG). This is in contrast to the low dose *LsAA9A*:Cell<sub>3</sub> structure where the Tyr-O distance is 2.47 Å (PDB 5ACF). Furthermore, the equatorial position in the low dose *LsAA9A*:Xyl<sub>5</sub> is occupied by a water molecule, not a chloride ion, as corroborated by the EPR spectroscopy. Thus, a mechanism by which a copper-bound superoxide is generated next to the substrate is possible within the *LsAA9A*-Xyl<sub>5</sub> complex. Such a mechanism may be expected to be rate-independent on the redox potential of the reducing agent, since the rate-limiting step is likely to be hydrogen atom abstraction by the superoxide from the substrate rather than reductive cleavage of the O-O bond. Therefore, the fact that the rate of cleavage of xylan and Xyl<sub>6</sub> by *LsAA9A* is less dependent on reducing agent while the cleavage of the other substrates is strongly dependent (Figure 4) illustrates that a different oxidative mechanism is in operation. Thus the extent of activity on certain substrates is a function of the oxidative species which can be formed at the copper ion which is—in turn—dependent on the substrate. This means that for some substrates the use of reducing agents with different potentials can profoundly affect apparent substrate specificity. But, more importantly, LPMOs appear to have more than one oxidative mechanism available for substrate cleavage, governed to some extent by the nature of the substrate-LPMO interaction. Indeed, the existence of multiple oxidative mechanisms for a single LPMO is an intriguing contribution to the on-going debate about LPMO mode of action. Results



424 obtained in this study broaden the known substrate specificity of AA9 LPMOs to include  
425 isolated xylan and xylo-oligosaccharides, and mannosyl-containing bonds within  
426 glucomannan. We further show that oxidation type (C1/C4) is influenced by substrate type,  
427 and in this work differed between oligo- and polysaccharides. This investigation into the  
428 molecular causes of AA9 LPMO substrate specificity demonstrated the existence of  
429 multiple influences. As with carbohydrate-acting hydrolases, for example, LPMO substrate  
430 specificity is dictated by binding cleft protein:carbohydrate interactions. But in addition, the  
431 fact that activity on some substrates is differentially responsive to reducing agent potential  
432 suggests that these carbohydrates do not properly activate the active site copper, and are  
433 cleaved through an alternative oxidative pathway. Combinations of canonical and non-  
434 canonical mechanisms greatly extend the range of potential substrates for LPMOs and  
435 offer new insight into their biochemical mode of action.

436

## 437 **Materials and methods**

### 438 *Phylogenetic tree*

439 AA9 is a family with more than 6000 sequences listed in NCBI nr and JGI databases in  
440 2016. Because of high variability in the N-terminal portion of LPMO amino acid sequences,  
441 no significant global alignment of LPMOs can be obtained – thereby limiting global  
442 downstream phylogenetic analyses. We chose therefore to extract the highly variable N-  
443 terminal half of these sequences (which includes two histidine residues involved in the  
444 coordination of the copper atom) for phylogenetic analysis as well as to limit the analysis to  
445 sequences that are closely related to each other and to those that have been  
446 biochemically characterized in the literature. We reduced the set of AA9 sequences to  
447 those that gave BLAST bit-scores greater than or equal to a value of 200, using *LsAA9A*  
448 and *TaAA9A* as queries. A Jaccard distance matrix was compiled from BLAST bit scores  
449 and represented as a tree, built according to the principle of neighbor-joining method<sup>44</sup>  
450 displaying the resulting 444 sequences (Fig. 1).

### 451 *Protein production*

452 Cloning, expression, and purification of *LsAA9A* was done as described previously<sup>33</sup>. The  
453 gene encoding *CvAA9A* was amplified from genomic DNA of *Collariella virescens*  
454 (formerly known as *Chaetomium virescens*) and expressed in *Aspergillus oryzae* MT3568.  
455 The secreted LPMO was purified using a Butyl Toyopearl resin followed by purification on  
456 a Q-Sepharose FF resin followed by ultrafiltration with 10 kDa cutoff filter.

### 457 *Enzyme assays*

458 Apo-*LsAA9A* and apo-*CvAA9A* were pre-incubated for 0.5–1 h at 5 °C in 0.9 stoichiometric  
459 Cu(II)(NO<sub>3</sub>)<sub>2</sub> immediately before enzyme reactions. AA9 enzyme reactions on  
460 oligosaccharides were in 10 µL containing 5 nmol oligosaccharide, 100 mM ammonium  
461 formate pH 6, ±4 mM ascorbate, pyrogallol or cysteine, ±5 pmol *LsAA9A* or *TaAA9A* and  
462 were incubated at 20 °C for 4 h. Xyloglucan endoglucanase (XEG) reactions were in 10 µL

containing 5 nmol oligosaccharide, 100 mM ammonium formate pH 6,  $\pm 10$   $\mu$ mol GH5 XEG and were incubated at 20 °C for 4 h. Oligosaccharides were purchased from Megazyme (see also following section). In general, enzyme reactions on polysaccharides were in 100  $\mu$ L containing 0.5% (w/v) polysaccharide, 100 mM ammonium formate pH 6,  $\pm 4$  mM ascorbate, pyrogallol or cysteine,  $\pm 63$  pmol LPMO, and were incubated at 20 °C for 16 h. Avicel cellulose was purchased from Sigma-Aldrich, UK; barley beta-glucan medium viscosity (mixed-linkage glucan), konjac glucomannan, tamarind xyloglucan, birchwood xylan, corn starch and laminarin were purchased from Megazyme, Ireland; squid-pen  $\beta$ -chitin was a kind gift from Dominique Gillet of Mahtani Chitosan. Phosphoric acid-swollen cellulose (PASC) was prepared as described previously<sup>33</sup>. Mixed-linkage glucan, glucomannan, xyloglucan, xylan, starch and laminarin were boiled for 5 mins to make solubilized 1% (w/v) stock solutions before reactions. To aid solubilisation where necessary, water was added to a methanol: polysaccharide slurry before boiling, which improved dispersion throughout the water. Reactions were routinely stopped by addition of three reaction volumes of 96% (v/v) ethanol before precipitation of the undigested substrates, and separation of the reaction products for further analysis. Polysaccharide Analysis by Carbohydrate Electrophoresis (PACE) using high concentration acrylamide gels (for resolution of small oligosaccharides) and lower concentration gels (for resolution of larger oligosaccharides) was carried out as described by Frandsen et al.<sup>33</sup> and Goubet et al.<sup>45</sup> respectively. MALDI-ToF MS was performed as described previously<sup>46</sup>. 2-Aminobenzamide (2-AB) labelling was performed as described previously<sup>33</sup>. All experiments were carried out at least three times.

Sodium borohydride reducing agent experiments were performed as described by Frandsen et al.<sup>33</sup>. HPAEC was performed on a CarboPac PA1 column (Dionex) with injections of 20  $\mu$ L and elution at 0.4 mL min<sup>-1</sup>. The elution profile was: 0–3 min, 10 mM NaOH (isocratic); 3–6 min, 10→1 mM NaOH (linear gradient); 6–19 min, 1 mM NaOH (isocratic); 19–37 min, 45 mM NaOH, 225 mM sodium acetate (isocratic). A pulsed amperometric detector (PAD) with a gold electrode was used. PAD response was calibrated using markers (500 pmol).

*X-ray crystallography and PDB database searches*

493 All crystallization trials were set up in MRC 2-well plates at room temperature using an  
 494 Oryx-8 robot (Douglas Instrument). Crystals were obtained by sitting-drop vapor diffusion  
 495 technique in drops of 0.3-0.5  $\mu$ L with a reservoir volume of 100  $\mu$ L. Pre-incubation with 1-2  
 496 mM Cu(II) acetate for 30-60 min was carried out for all crystallization trials. Crystallization  
 497 and post-crystallization experimental details are shown in Supplementary Table 4. Crystals  
 498 were cryocooled in liquid nitrogen and all datasets were collected at cryogenic  
 499 temperatures (100 K) at either the MX beamlines I911-2/I911-3 at MAX-lab in Lund,  
 500 Sweden, or at the MX beamlines ID23-1, ID23-2 or ID30-B at ESRF, Grenoble, France  
 501 (Supplementary Table 5). *LsAA9A* crystallization was performed as described in Frandsen  
 502 et al.<sup>33</sup>. Oligosaccharide substrates used for soaking were purchased from Megazyme  
 503 (MLG (G4G4G3G and G4G3G4G), xylotriose (Xyl<sub>3</sub>), xylotetraose (Xyl<sub>4</sub>), xylopentaose  
 504 (Xyl<sub>5</sub>), xyloglucan heptasaccharide (XXXG), cellotriose (Cell<sub>3</sub>) or provided by Novozymes  
 505 A/S (cellopentaose (Cell<sub>5</sub>)). Data were initially collected on crystals soaked with G4G4G3G  
 506 (*LsAA9A*:G4G4G3G; PDB 5NLR), Xyl<sub>3</sub> (*LsAA9A*:Xyl<sub>3</sub>; PDB 5NLQ), Xyl<sub>4</sub> (*LsAA9A*:Xyl<sub>4</sub>;  
 507 PDB 5NLP) and Cell<sub>5</sub> (*LsAA9A*:Cell<sub>5</sub>; 5NLS). On a crystal soaked with Xyl<sub>5</sub> a dataset with  
 508 reduced X-ray dose ((*LsAA9A*:Xyl<sub>5</sub>Cu(II); PDB 5NLN; 40 frames of 5.7% transmission,  
 509 0.05s exposure/frame, 1° oscillation with a beamsize of 10x10  $\mu$ m) was collected using  
 510 helical collection to minimize photoreduction of the active site copper. Subsequently, on  
 511 similar crystals another full dose dataset was collected to high resolution (*LsAA9A*:Xyl<sub>5</sub>;  
 512 PDB 5NLO). Ladders of glucomannan (GM), from konjac, and of xyloglucan (XG), from  
 513 tamarind, were prepared by partial acid hydrolysis (20-200 mM TFA for 20 min at 120°C)  
 514 of polysaccharide substrates purchased from Megazyme. Hydrolyzed products were  
 515 isolated using ethanol precipitation to remove the remaining polysaccharides. The  
 516 oligosaccharides were dried thoroughly using a SpeedVac. Data were collected on crystals  
 517 soaked in GM (*LsAA9A*:GM; PDB 5NKW) or XG stock solutions (in 3.8 M NaCl, 0.1 M  
 518 citric acid pH 5.5). Crystals were also soaked in the presence of 0.3 M XXXG, and up to  
 519 1.2 M of XG oligosaccharide purchased from Megazyme (consisting primarily of  
 520 XXXGXXXG, see Courtade et al.<sup>21</sup>). No complex structures were obtained from any of the  
 521 crystals soaked with XG substrates, either because no binding was observed or only  
 522 cellooligosaccharides were bound (presumably because acid hydrolysis caused  
 523 debranching).

CvAA9A was deglycosylated in 20 mM MES, pH 6.0, 125 mM NaCl by incubation with approximately 0.03 units mg<sup>-1</sup> CvAA9A of endoglycosidase H from (Roche Diagnostics, 11643053001), and then buffer exchanged to 20 mM Na-acetate pH 5.5. Intergrown crystals were initially obtained in an index screen in conditions of 1.5–2.0 M (NH<sub>4</sub>)<sub>2</sub>SO<sub>4</sub> (and in some cases 0.1 M NaCl) in pH 6.5–8.5 (0.1 M of either Bis-Tris, HEPES or Tris). The crystals diffracted to 2.0–3.5 Å resolution but were multiple. Crystal conditions were optimized in a range of 1.2 M – 2.6 M (NH<sub>4</sub>)<sub>2</sub>SO<sub>4</sub> (+/- 0.1 M NaCl) in pH 6.5–8.5, which produced crystal plates suitable for mounting. A dataset collected at I911-3 on a crystal grown in 0.1 M Bis-Tris pH 6.5, 2.0 M (NH<sub>4</sub>)<sub>2</sub>SO<sub>4</sub> could be processed in *P*2<sub>1</sub> to 2.5 Å (PDB 5NLT). A preliminary CvAA9A structure with four molecules in the asymmetric unit was solved by Molecular Replacement using MOLREP with modified coordinates of the high resolution structure of LsAA9A (PDB 5ACH) which is 41% identical, as a model and refined isotropically to an R<sub>free</sub> of 32%. From another dataset (collected on a crystal grown in presence of 0.1 M NaCl; Supplementary Table 4) a structure solved (using the preliminary one) with six molecules in the asymmetric unit could be fully modelled and refined resulting in the complete CvAA9A structure (Supplementary Table 5). The 6 molecules in the asymmetric unit are very similar (average RMSDs of 0.08Å). The density of MeHis1 is less clear in chains C and F, and in particular methylation is not as obvious in all chains. Soaks (with 1.2 M Cell<sub>3</sub>) of CvAA9A were also prepared. Data were collected to 2.1 Å and the electron density showed a Cell<sub>3</sub> molecule, which however was not bound at the active site (not shown). Soaks with Cell<sub>6</sub> damaged the crystals.

Each dataset was processed using XDS (the resolution cutoff was chosen on the basis of a CC<sub>1/2</sub> around 50%) and subsequently scaled using XSCALE. Refmac5 was used for restrained refinement of the structures in which LsAA9A:Xyl<sub>5</sub> was refined anisotropically, while LsAA9A:Xyl<sub>3</sub> was refined anisotropically for protein atoms and isotropically for all other atoms. All other structures were refined isotropically for all atoms. For LsAA9A:G4G4G3G the structure was best modelled by the G4G4G portion of the substrate bound mainly in subsite -1 to +2 (80% occupancy) and with a minor conformation occupying subsite -2 to +1 (20% occupancy). Near subsite -2 a number of water molecules were modelled with 80% occupancy. Ligands and structures were modelled in COOT and validated using MolProbity (within COOT) and Procheck (CCP4 suite) which reported Ramachandran plots with 99% of residues in allowed regions for all

structures. Scaled data statistics and refinement statistics are summarized in Supplementary Table 5.

To identify potential stacking interactions of the  $\beta$ -face of  $\beta$ -mannose with His, the PDB database was searched with Glyvicinity<sup>47</sup>. First all protein/ $\beta$ -mannose interactions within a distance cut-off of 4.0 Å for structures determined at a resolution better than 3.0 Å were identified. Among these, only two structures were found where the interactions involved His residues and the pyranose O5. The interactions between the imidazole and the pyranose rings were side by side or almost perpendicular, and thus not comparable with the +1 subsite interactions of the *LsAA9A* complexes.

### *Electron Paramagnetic Resonance (EPR) Spectroscopy*

Continuous wave (cw) X-band frozen solution EPR spectra of 0.2 to 0.3 mM solution of *LsAA9A* or *CvAA9A* (in 10% v/v glycerol) at pH 6.0 (50 mM sodium phosphate buffer with or without addition of 200 mM NaCl or 20 mM MES buffer, 200 mM NaCl) and 165 K were acquired on a Bruker EMX spectrometer operating at ~9.30 GHz, with modulation amplitude of 4 G, modulation frequency 100 kHz and microwave power of 10.02 mW (3 scans). Avicel cellulose, konjac glucomannan, tamarind xyloglucan and birchwood xylan were added to the EPR tube containing the protein as solids. Alternatively, glucomannan and xylan were heated until dissolution (ca. 2 min) to make solubilized 1% (w/v) stock solutions in water, which were then used for addition of excess polysaccharide to *LsAA9A*. Cellohexaose and xylohexaose were added to the protein solution either from stock solutions in water or as a solid up to 60 or 150-fold excess, respectively. For the experiments in the presence of xylohexaose, additional NaCl was added to the protein alone or the protein:Xyl<sub>6</sub> mixture from a 5 M stock solution. Due to the high amount of protein required by the technique, the data presented are from single EPR experiments, although the spectra with Cell<sub>6</sub>, Xyl<sub>6</sub> and avicel were performed in at least duplicate.

Spectral simulations were carried out using EasySpin 5.0.3<sup>48</sup> integrated into MATLAB R2016a<sup>49</sup> software on a desktop PC. Simulation parameters are given in Table 2.  $g_z$  and  $|A_z|$  values were determined accurately from the absorptions at low field. It was assumed that  $g$  and  $A$  tensors were axially coincident.

## Data availability

Protein Data Bank: Atomic coordinates and structure factors for the reported crystal structures were deposited under accession codes 5NLT (CvAA9A), 5NLS (LsAA9A-Cell<sub>5</sub>), 5NLR (LsAA9A-G4G4G3G), 5NKG (LsAA9A-GM), 5NLQ (LsAA9A-Xyl<sub>3</sub>), 5NLP (LsAA9A-Xyl<sub>4</sub>), 5NLO (LsAA9A-Xyl<sub>5</sub>) and 5NLN (LsAA9A-Xyl<sub>5</sub>-Cu<sub>II</sub>), GenBank: Sequence data for CvAA9A were deposited under accession code KY884985. Raw EPR data are available on request through the Research Data York (DOI: 10.15124/5810c962-148c-4328-ab92-895e2dae4d3c).

## References

- 1 Carroll, A. & Somerville, C. Cellulosic Biofuels. *Annu. Rev. Plant Biol.* **60**, 165-182, (2009).
- 2 Perlack, R. D. & Stokes, B. J., Leads. *U.S. Billion-Ton Update: Biomass Supply for a Bioenergy and Bioproducts Industry*. Technical Report ORNL/TM-2011/224, 227. (U.S. Department of Energy, Oak Ridge National Laboratory, Oak Ridge, TN, 2011).
- 3 Marriott, P. E., Gomez, L. D. & McQueen-Mason, S. J. Unlocking the potential of lignocellulosic biomass through plant science. *New Phytol.* **209**, 1366-1381, (2016).
- 4 Simmons, T. J. *et al.* Folding of xylan onto cellulose fibrils in plant cell walls revealed by solid-state NMR. *Nat. Commun.* **7**, (2016).
- 5 Correa, T. L. R., dos Santos, L. V. & Pereira, G. A. G. AA9 and AA10: from enigmatic to essential enzymes. *Appl. Microbiol. Biot.* **100**, 9-16, (2016).
- 6 Muller, G., Varnai, A., Johansen, K. S., Eijsink, V. G. H. & Horn, S. J. Harnessing the potential of LPMO-containing cellulase cocktails poses new demands on processing conditions. *Biotechnol. Biofuels* **8**, (2015).
- 7 Hemsworth, G. R., Henrissat, B., Davies, G. J. & Walton, P. H. Discovery and characterization of a new family of lytic polysaccharide monooxygenases. *Nat. Chem. Biol.* **10**, 122-126, (2014).
- 8 Cantarel, B. L. *et al.* The Carbohydrate-Active EnZymes database (CAZy): an expert resource for Glycogenomics. *Nucleic Acids Res.* **37**, D233-D238, (2009).
- 9 Lombard, V., Ramulu, H. G., Drula, E., Coutinho, P. M. & Henrissat, B. The carbohydrate-active enzymes database (CAZy) in 2013. *Nucleic Acids Res.* **42**, D490-D495, (2014).
- 10 Vu, V. V., Beeson, W. T., Span, E. A., Farquhar, E. R. & Marletta, M. A. A family of starch-active polysaccharide monooxygenases. *P. Natl. Acad. Sci. USA* **111**, 13822-13827, (2014).
- 11 Lo Leggio, L. *et al.* Structure and boosting activity of a starch-degrading lytic polysaccharide monooxygenase. *Nat. Commun.* **6**, (2015).
- 12 Quinlan, R. J. *et al.* Insights into the oxidative degradation of cellulose by a copper metalloenzyme that exploits biomass components. *P. Natl. Acad. Sci. USA* **108**, 15079-15084, (2011).
- 13 Hemsworth, G. R., Johnston, E. M., Davies, G. J. & Walton, P. H. Lytic Polysaccharide Monooxygenases in Biomass Conversion. *Trends Biotechnol.* **33**, 747-761, (2015).
- 14 Vaaje-Kolstad, G., Horn, S. J., van Aalten, D. M. F., Synstad, B. & Eijsink, V. G. H. The non-catalytic chitin-binding protein CBP21 from *Serratia marcescens* is essential for chitin degradation. *J. Biol. Chem.* **280**, 28492-28497, (2005).

629 15 Merino, S. T. & Cherry, J. Progress and challenges in enzyme development for Biomass utilization.  
630 *Adv. Biochem. Eng. Biot.* **108**, 95-120, (2007).

631 16 Harris, P. V. *et al.* Stimulation of Lignocellulosic Biomass Hydrolysis by Proteins of Glycoside  
632 Hydrolase Family 61: Structure and Function of a Large, Enigmatic Family. *Biochemistry-Us* **49**,  
633 3305-3316, (2010).

634 17 Vaaje-Kolstad, G. *et al.* An Oxidative Enzyme Boosting the Enzymatic Conversion of Recalcitrant  
635 Polysaccharides. *Science* **330**, 219-222, (2010).

636 18 Isaksen, T. *et al.* A C4-oxidizing Lytic Polysaccharide Monooxygenase Cleaving Both Cellulose and  
637 Cello-oligosaccharides. *J. Biol. Chem.* **289**, 2632-2642, (2014).

638 19 Agger, J. W. *et al.* Discovery of LPMO activity on hemicelluloses shows the importance of oxidative  
639 processes in plant cell wall degradation. *P. Natl. Acad. Sci. USA* **111**, 6287-6292, (2014).

640 20 Bennati-Granier, C. *et al.* Substrate specificity and regioselectivity of fungal AA9 lytic polysaccharide  
641 monooxygenases secreted by *Podospora anserina*. *Biotechnol. Biofuels* **8**, (2015).

642 21 Courtade, G. *et al.* Backbone and side-chain H-1, C-13, and (15) N chemical shift assignments for the  
643 apo-form of the lytic polysaccharide monooxygenase NcLPMO9C. *Biomol. NMR Assign.* **10**, 277-280,  
644 (2016).

645 22 Jagadeeswaran, G., Gainey, L., Prade, R. & Mort, A. J. A family of AA9 lytic polysaccharide  
646 monooxygenases in *Aspergillus nidulans* is differentially regulated by multiple substrates and at  
647 least one is active on cellulose and xyloglucan. *Appl. Microbiol. Biot.* **100**, 4535-4547, (2016).

648 23 Frommhagen, M. *et al.* Discovery of the combined oxidative cleavage of plant xylan and cellulose by  
649 a new fungal polysaccharide monooxygenase. *Biotechnol. Biofuels* **8**, (2015).

650 24 Levasseur, A., Drula, E., Lombard, V., Coutinho, P. M. & Henrissat, B. Expansion of the enzymatic  
651 repertoire of the CAZy database to integrate auxiliary redox enzymes. *Biotechnol. Biofuels* **6**,  
652 (2013).

653 25 Yakovlev, I. *et al.* Substrate-specific transcription of the enigmatic GH61 family of the pathogenic  
654 white-rot fungus *Heterobasidion irregulare* during growth on lignocellulose. *Appl. Microbiol. Biot.*  
655 **95**, 979-990, (2012).

656 26 Poidevin, L. *et al.* Comparative analyses of *Podospora anserina* secretomes reveal a large array of  
657 lignocellulose-active enzymes. *Appl. Microbiol. Biot.* **98**, 7457-7469, (2014).

658 27 Frommhagen, M. *et al.* Lytic polysaccharide monooxygenases from *Myceliophthora thermophila* C1  
659 differ in substrate preference and reducing agent specificity. *Biotechnol. Biofuels* **9**, (2016).

660 28 Kracher, D. *et al.* Extracellular electron transfer systems fuel cellulose oxidative degradation.  
661 *Science* **352**, 1098-1101, (2016).

662 29 Borisova, A. S. *et al.* Structural and Functional Characterization of a Lytic Polysaccharide  
663 Monooxygenase with Broad Substrate Specificity. *J. Biol. Chem.* **290**, 22955-22969, (2015).

664 30 Frandsen, K. E. H. & Lo Leggio, L. Lytic polysaccharide monooxygenases: a crystallographer's view  
665 on a new class of biomass-degrading enzymes. *Isucrj* **3**, 448-467, (2016).

666 31 Vaaje-Kolstad, G., Forsberg, Z., Loose, J. S., Bissaro, B. & Eijsink, V. G. Structural diversity of lytic  
667 polysaccharide monooxygenases. *Curr Opin Struct Biol* **44**, 67-76, (2017).

668 32 Davies, G. J., Wilson, K. S. & Henrissat, B. Nomenclature for sugar-binding subsites in glycosyl  
669 hydrolases. *Biochem J* **321 ( Pt 2)**, 557-559, (1997).

670 33 Frandsen, K. E. H. *et al.* The molecular basis of polysaccharide cleavage by lytic polysaccharide  
671 monooxygenases. *Nat. Chem. Biol.* **12**, 298+, (2016).

672 34 Walton, P. H. & Davies, G. J. On the catalytic mechanisms of lytic polysaccharide monooxygenases.  
673 *Curr. Opin. Chem. Biol.* **31**, 195-207, (2016).

674 35 Cannella, D. *et al.* Light-driven oxidation of polysaccharides by photosynthetic pigments and a  
675 metalloenzyme. *Nat. Commun.* **7**, (2016).

676 36 Lenfant, N. *et al.* A bioinformatics analysis of 3400 lytic polysaccharide oxidases from family AA9.  
677 *Carbohydr Res*, (2017).



- 37 Loose, J. S. M. *et al.* Activation of bacterial lytic polysaccharide monooxygenases with cellobiose dehydrogenase. *Protein Sci.* **25**, 2175-2186, (2016).
- 38 Frandsen, K. E. H., Poulsen, J. C. N., Tovborg, M., Johansen, K. S. & Lo Leggio, L. Learning from oligosaccharide soaks of crystals of an AA13 lytic polysaccharide monooxygenase: crystal packing, ligand binding and active-site disorder. *Acta Crystallogr. D.* **73**, 64-76, (2017).
- 39 Kojima, Y. *et al.* A Lytic Polysaccharide Monooxygenase with Broad Xyloglucan Specificity from the Brown-Rot Fungus *Gloeophyllum trabeum* and Its Action on Cellulose-Xyloglucan Complexes. *Appl. Environ. Microb.* **82**, 6557-6572, (2016).
- 40 Nekiunaite, L., Arntzen, M. O., Svensson, B., Vaaje-Kolstad, G. & Abou Hachem, M. Lytic polysaccharide monooxygenases and other oxidative enzymes are abundantly secreted by *Aspergillus nidulans* grown on different starches. *Biotechnol. Biofuels* **9**, (2016).
- 41 Fanuel, M. *et al.* The *Podospora anserina* lytic polysaccharide monooxygenase PaLPMO9H catalyzes oxidative cleavage of diverse plant cell wall matrix glycans. *Biotechnol Biofuels* **10**, 63, (2017).
- 42 Asensio, J. L., Arda, A., Canada, F. J. & Jimenez-Barbero, J. Carbohydrate-Aromatic Interactions. *Accounts Chem. Res.* **46**, 946-954, (2013).
- 43 Kjaergaard, C. H. *et al.* Spectroscopic and computational insight into the activation of O-2 by the mononuclear Cu center in Polysaccharide monooxygenases. *Abstr. Pap. Am. Chem. S.* **248**, (2014).
- 44 Lefort, V., Desper, R. & Gascuel, O. FastME 2.0: A Comprehensive, Accurate, and Fast Distance-Based Phylogeny Inference Program. *Mol. Biol. Evol.* **32**, 2798-2800, (2015).
- 45 Goubet, F., Jackson, P., Deery, M. J. & Dupree, P. Polysaccharide analysis using carbohydrate gel electrophoresis: A method to study plant cell wall polysaccharides and polysaccharide hydrolases. *Anal. Biochem.* **300**, 53-68, (2002).
- 46 Tryfona, T. *et al.* Carbohydrate structural analysis of wheat flour arabinogalactan protein. *Carbohydr. Res.* **345**, 2648-2656, (2010).
- 47 Rojas-Macias, M. A. & Lutteke, T. Statistical analysis of amino acids in the vicinity of carbohydrate residues performed by GlyVicinity. *Methods Mol Biol* **1273**, 215-226, (2015).
- 48 Stoll, S. & Schweiger, A. EasySpin, a comprehensive software package for spectral simulation and analysis in EPR. *J Magn Reson* **178**, 42-55, (2006).
- 49 MATLAB and Statistics Toolbox Release 2014a (The MathWorks, I., Natick, Massachusetts, United States).

## Acknowledgements

We wish to thank MAXLAB, Sweden and the European Synchrotron Radiation Facility (ESRF), France, for synchrotron beamtime and assistance. Travel to synchrotrons was supported by the Danish Ministry of Higher Education and Science through the Instrument Center DANSCATT and the European Community's Seventh Framework Programme (FP7/2007-2013) under BioStruct-X (grant agreement 283570).

This work was supported by the UK Biotechnology and Biological Sciences Research Council (grant numbers BB/L000423/1 to P.D. and P.H.W., and BB/L021633/1 to P.H.W.) and the Danish Council for Strategic Research (grant numbers 12-134923 to L.L.L. and 12-134922 to K.S.J.).

## **Author contributions**

T.J.S. carried out most of the activity assays, assisted by T.T. and L.F.L.W. K.E.H.F. carried out most of the structural studies with J.C.P., T.T. and L.L.L. L.C. carried out EPR spectroscopy. L.N. and B.H. carried out phylogenetic studies. M.T. and K.S. carried out target protein identification and production. P.D., L.L.L. and P.W. supervised the experimental work. T.J.S., K.E.H.F., K.S.J.O., P.W., L.L.L. and P.D. analysed the data and wrote the paper.

## **Competing Financial Interests**

M.T. and K.S. are employees of Novozymes, a producer of enzymes for industrial use.

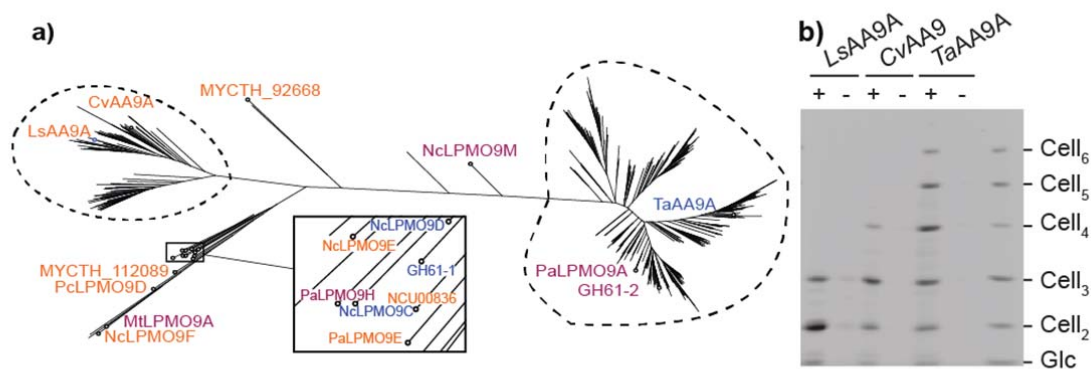


**Figure 1: Sequence similarity between *LsAA9A*, *CvAA9A* and *TaAA9A* and analysis of their reaction products.** **a**, Distance tree of 444 selected AA9 sequences (see methods). Blue, purple and orange labels designate AA9 enzymes that oxidize the sugar ring at C1, C4 and C1+C4, respectively. See Supplementary Table 1 for protein accession numbers. Unlabelled branches represent AA9 enzymes for which the regioselectivity of oxidation is not available from the literature. **b**, PACE gel showing reaction products of the three enzymes on PASC; +, incubation with 4mM ascorbate; -, incubation without ascorbate (performed in triplicate).

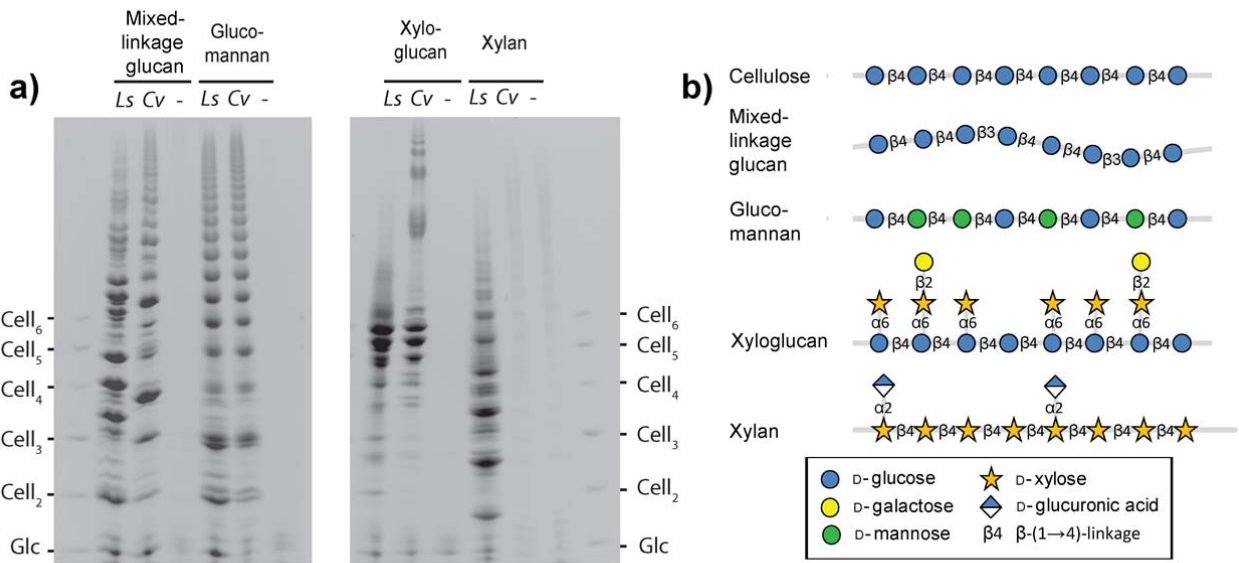


**Figure 2: Comparison of *LsAA9A* and *CvAA9A* action on non-cellulosic substrates.**

**a**, PACE gel showing digestion products on lignocellulosic polysaccharides with 4mM ascorbate reducing agent. *Ls*, *LsAA9A*; *Cv*, *CvAA9A*; -, no enzyme. **b**, Structures of polysaccharides.

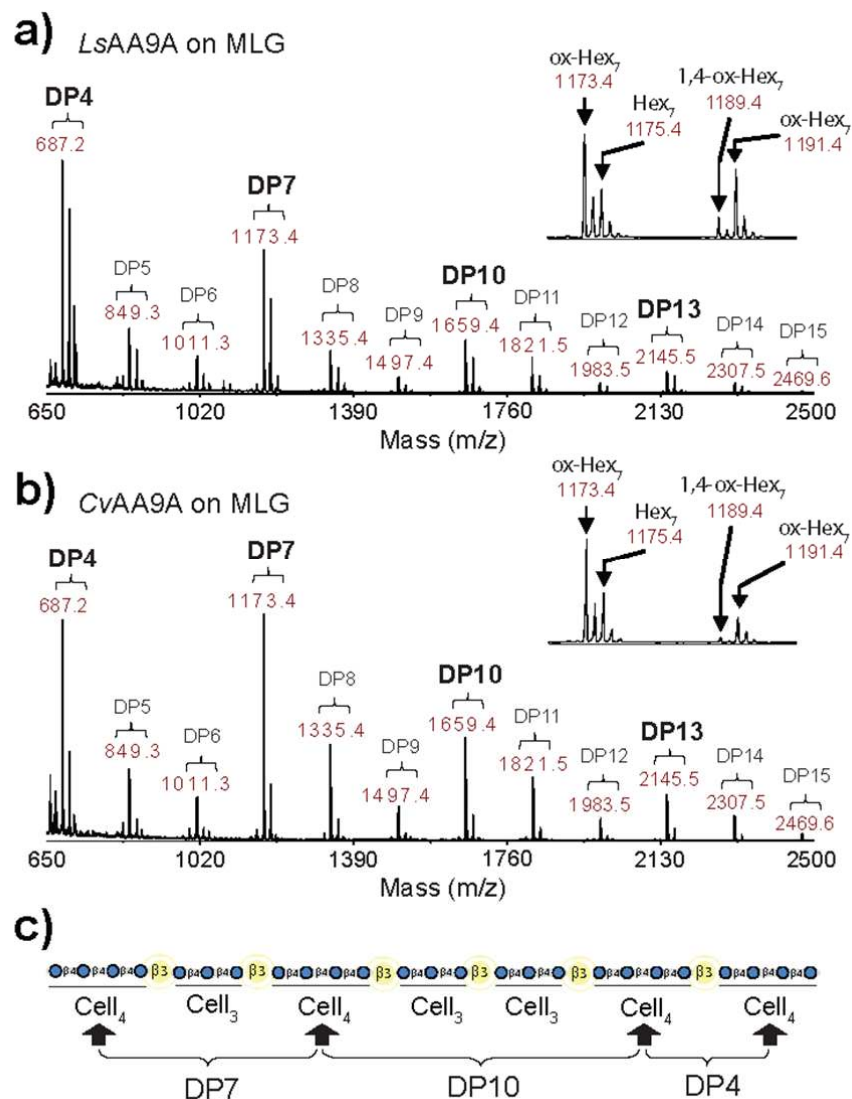


**Figure 3: *LsAA9A* and *CvAA9A* digestion products of MLG suggest preference for *Cell*<sub>4</sub> region cleavage.** Products of *LsAA9A* (a) and *CvAA9A* (b) activity on barley MLG with 4mM ascorbate were analysed by MALDI-ToF MS. Both enzymes can produce both C1 and C4 oxidation on MLG (1,4-ox; oxidized C1 and C4. See insets). Further, oligosaccharide profiles show a distinct pattern indicative of the mechanism of attack and substrate specificity of each enzyme on MLG. c, proposed region of cleavage.

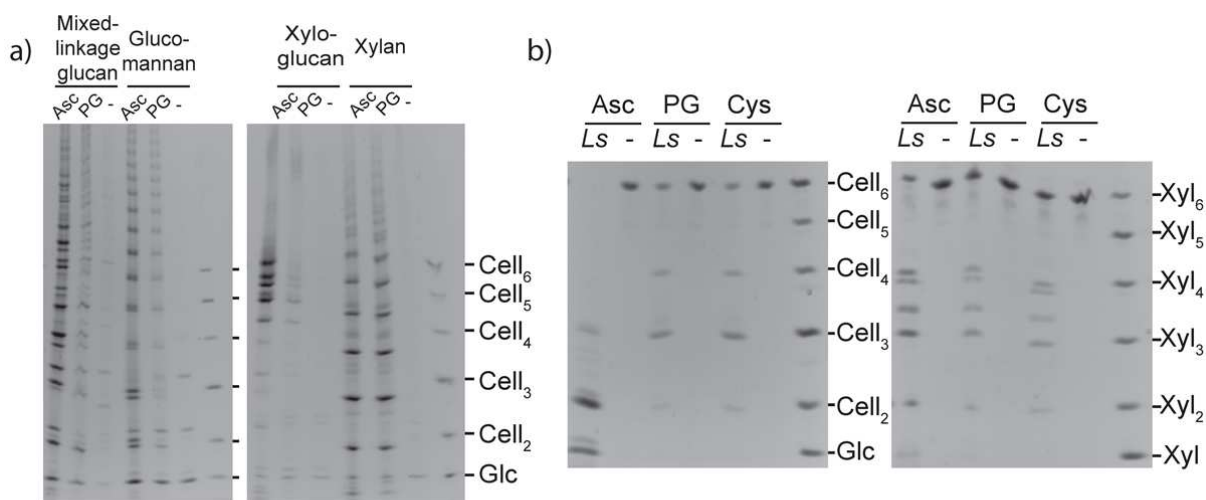
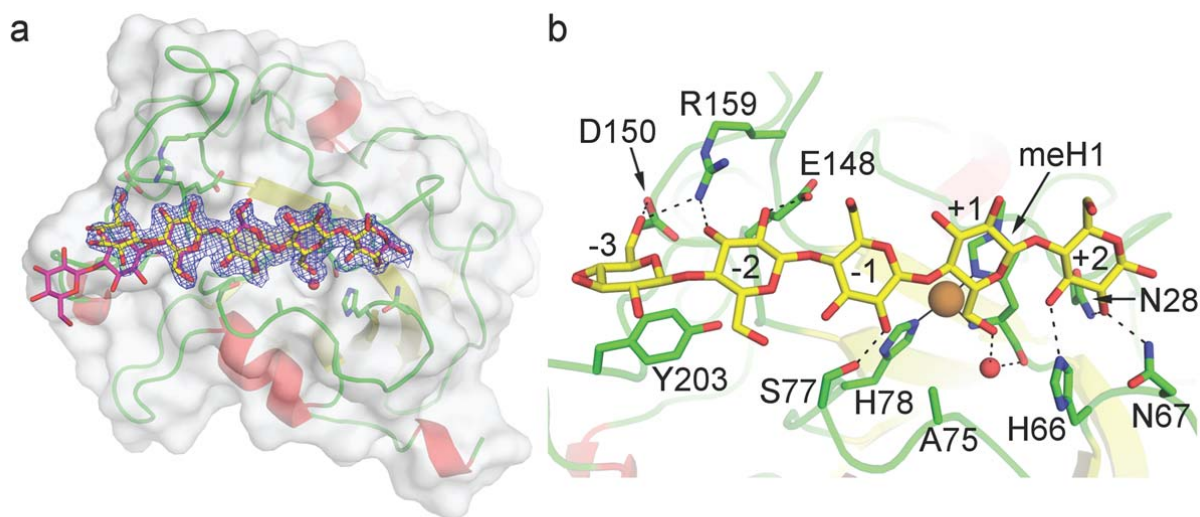


**Figure 4: *LsAA9A* activity on different poly- and oligosaccharide substrates show differing sensitivity to reducing agent potential.** a, PACE gels showing products of *LsAA9A* activity on MLG, glucomannan, xyloglucan and xylan polysaccharides using 4mM ascorbate or 4mM pyrogallol as reductants. The migration standards are cello oligosaccharides. b, PACE gels showing products of *LsAA9A* activity on Cell<sub>6</sub> and Xyl<sub>6</sub> oligosaccharides using 4mM ascorbate, pyrogallol and cysteine as reductants. Asc, Ascorbate; PG, pyrogallol; Cys, cysteine.



765

766 **Figure 5: *LsAA9A*:Cell<sub>5</sub> structure shows interactions at subsites -3 to +2.** a, Cell<sub>5</sub>  
 767 (yellow) is well defined in subsites -3 to +2. A 2F<sub>obs</sub>-F<sub>calc</sub> electron density map is shown at  
 768 1σ contour level. The structure shows no crystal contact induced distortion of the Cell<sub>5</sub>  
 769 substrate when compared to Cell<sub>6</sub> (magenta). b, *LsAA9A*-Cell<sub>5</sub> interactions are shown as  
 770 dashes. An additional interaction between subsite -3 (O)6 and Asp150 is gained in the  
 771 absence of symmetry related contacts to the substrate.

772



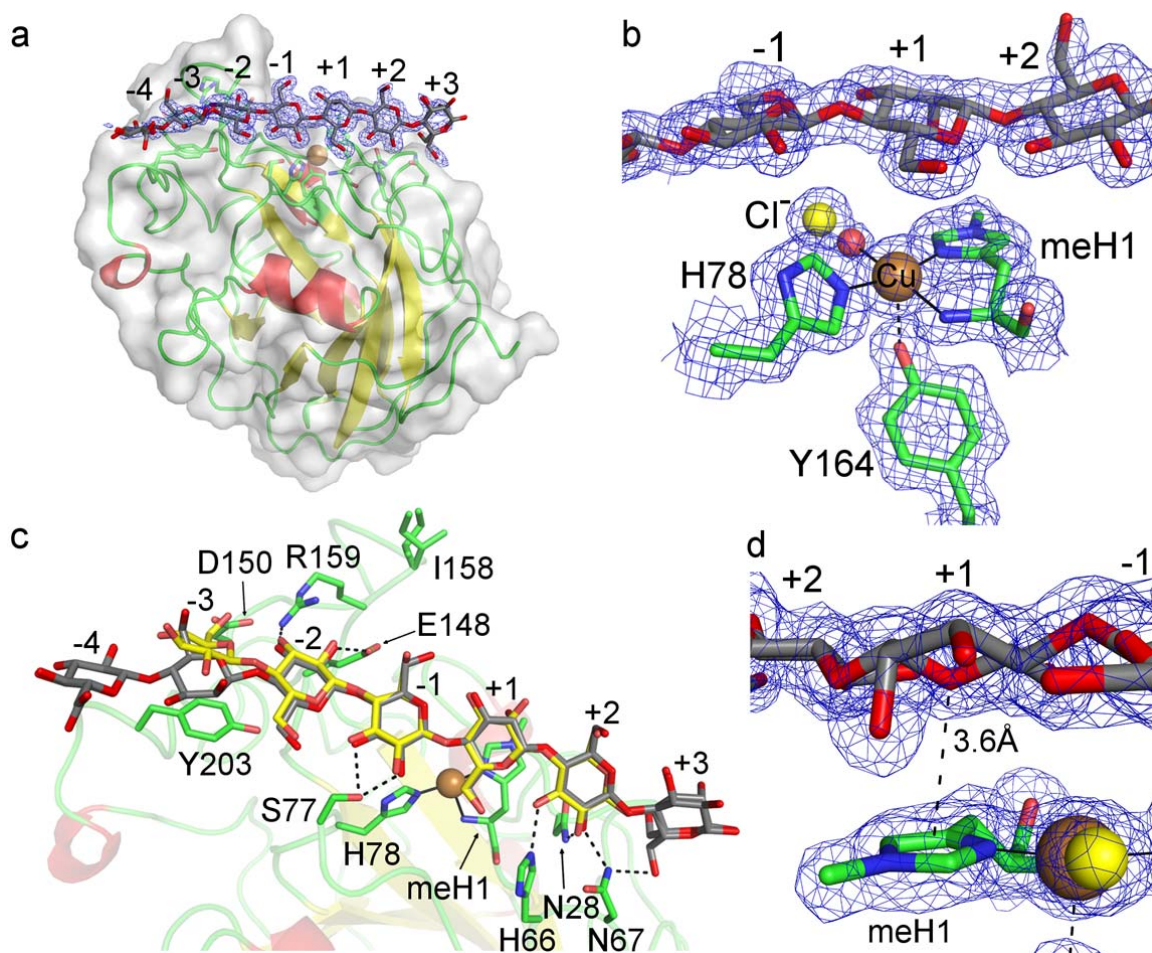


**Figure 6: Structure of the *LsAA9A*:glucomannan oligosaccharide complex.** **a**, Overall structure of *LsAA9A* with GM (blue) bound from subsite -4 to +3. **b**, Close up of the active site with GM fragment bound at subsite -1 to +2. Axial coordinations are in black dashes while equatorial coordinations are in full black lines. **c**, Top-down view of *LsAA9A*:GM (GM in grey) and for comparison *LsAA9A*:Cell<sub>5</sub> (Cell<sub>5</sub> in yellow). Dashed lines show interactions within hydrogen bond distance (2.8 Å). **d**, The C2-hydroxyl of mannose is clearly visible in the density at subsite +1. The pyranose O5-imidazole ring interaction (3.6 Å) is indicated with dashes. The interaction of MeHis and the mannosyl residue is very similar to the interaction with glucosyl residues in previous complexes<sup>38</sup>. A  $2F_{\text{obs}} - F_{\text{calc}}$  electron density map is shown at  $1\sigma$  contour level for panels a, b and d.



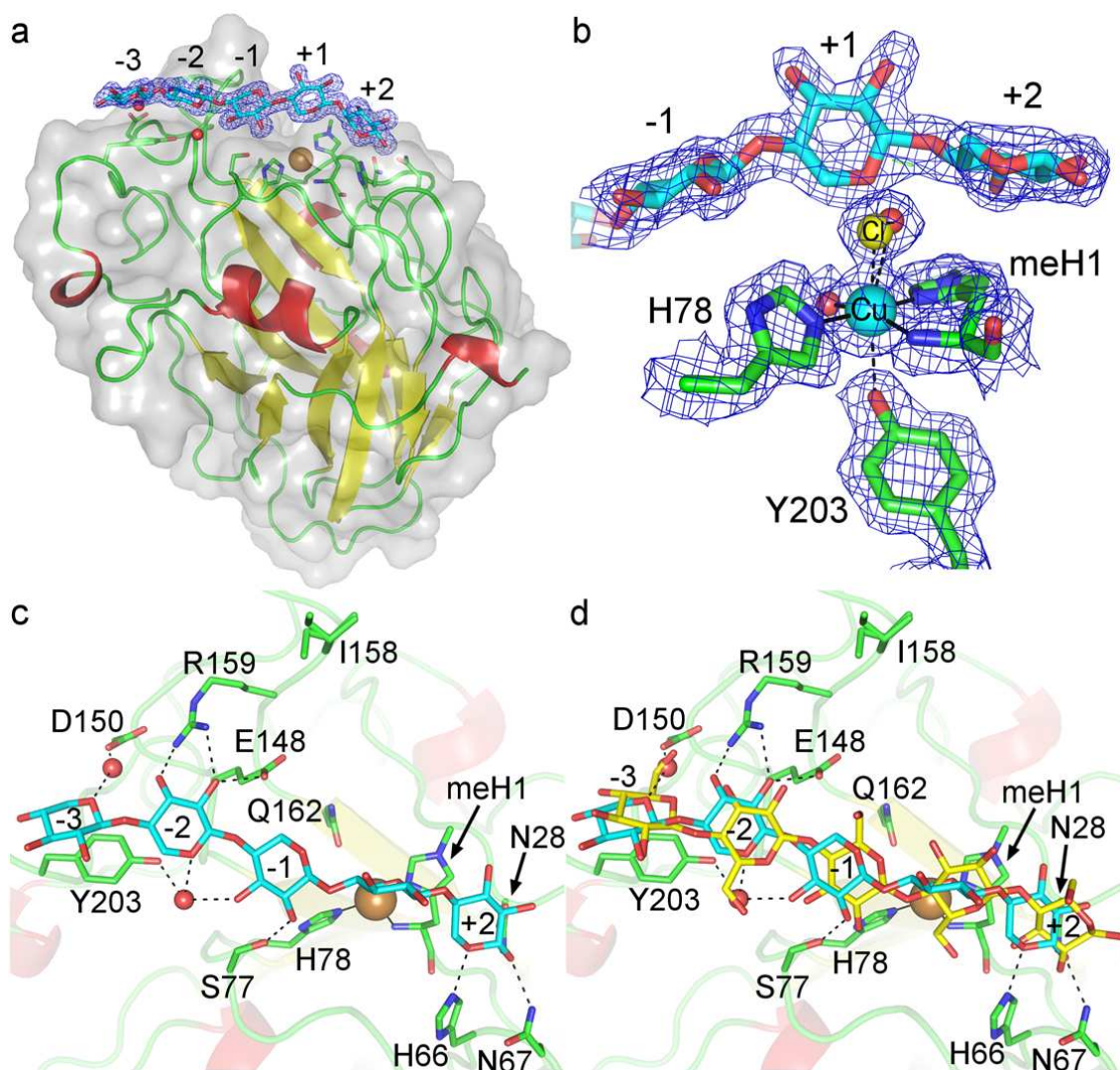


**Figure 7: Structure of the *LsAA9A*:xylo-oligosaccharide complex.** **a**, *LsAA9A*:Xyl<sub>5</sub> with bound substrate (in cyan) from subsite -3 to +2. **b**, Active site structure in the low dose *LsAA9A*:Xyl<sub>5</sub> structure, showing that the +1 xylosyl unit does not direct interact with the enzyme or displace the axial ligand on the copper (modelled as chloride and water in 0.5:0.5 ratio). **c**, Top-down view *LsAA9A*:Xyl<sub>5</sub> (in cyan). **d**, Top-down view *LsAA9A*:Xyl<sub>5</sub> (in cyan) and *LsAA9A*:Cell<sub>5</sub> (in yellow) shown for comparison. A  $2F_{\text{obs}} - F_{\text{calc}}$  electron density map is shown at 1 $\sigma$  contour level in panels a and b.

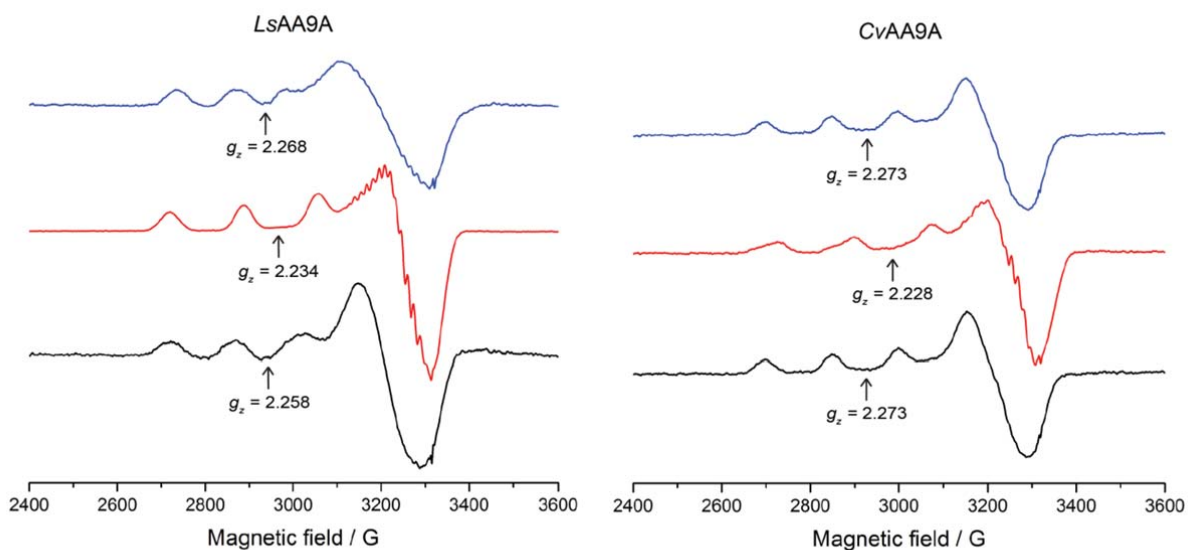


**Figure 8: X band cw EPR spectra of LsAA9A (left) and CvAA9A (right), 150 K.** Spectra were collected in the presence of 1 M NaCl (black), Cell<sub>6</sub> and 200 mM NaCl (red), or Xyl<sub>6</sub> and 1 M NaCl (blue).

| Polysaccharide                       | LsAA9A   |   | CvAA9    |   |
|--------------------------------------|----------|---|----------|---|
|                                      | Activity | Notes   | Activity | Notes   |
| Cellulose and cello-oligosaccharides | ++       | Activity on both cellulose oligosaccharides and insoluble cellulose material (PASC).  | ++       | Activity on both cellulose oligosaccharides and insoluble cellulose material (PASC).  |
| MLG                                  | ++       | Pattern suggests $\beta$ -(1 $\rightarrow$ 3)-bonds accommodated at specific places within active site, but not between -1 and +1.  | ++       | Pattern suggests $\beta$ -(1 $\rightarrow$ 3)-bonds accommodated at specific places within active site, but not between -1 and +1.  |
| Glucomannan and Man <sub>6</sub>     | ++       | Cleavage can occur with Glc or mannose at -1 or +1. Inactivity on Man <sub>6</sub> indicates some Glc C2 hydroxyl orientation needs to be present between -3 and +3.                        | ++       | Cleavage can occur with Glc or mannose at -1 or +1. Inactivity on Man <sub>6</sub> indicates some Glc C2 hydroxyl orientation needs to be present between -3 and +3.        |
| Xyloglucan                           | ++       | Cleavage occurs with unsubstituted Glc at subsite +1. Xylosyl substitution at -3, -2, -1, +2 and +3. Galactosyl-xylosyl substitutions can occur at either -2, -1 and/or +3.                 | ++       | Cleavage occurs with unsubstituted Glc at subsite +1. Xylosyl substitution at -3, -2, -1, +2 and +3. Galactosyl-xylosyl substitutions can occur at either -2, -1 and/or +3. |
| Xylan and Xyl <sub>6</sub>           | +        | Activity on both. Weak Xyl <sub>6</sub> activity compared to Cell <sub>6</sub> suggests that, while Glc C6 is not required for activity, it is very important at certain sites, such as +1. | +/-      | Much poorer activity of CvAA9A compared with LsAA9A.  |
| Starch                               | -        | Absence of activity indicates that LsAA9A necessarily cleaves $\beta$ -(1 $\rightarrow$ 4)-bonds.   | -        | Absence of activity indicates that CvAA9A necessarily cleaves $\beta$ -(1 $\rightarrow$ 4)-bonds.   |
| Laminarin                            | -        |   | -        |   |
| G4G3G4G (MLG oligosaccharide)        | -        |   | -        |   |
| Chitin                               | -        | Absence of activity indicates that LsAA9A either requires O2 interactions or cannot accommodate N-Acetyl on amino C2.   | -        | Absence of activity indicates that CvAA9A either requires O2 interactions or cannot accommodate N-Acetyl on amino C2.   |

798 **Table 1: Summary of activity assays on different substrates.** Semi-quantitative activity  
799 results summarising the activity of *LsAA9A* and *CvAA9A* on the range of different  
800 substrates used in this manuscript.

801

| Enzyme-substrate combination              | $g_z$ | $A_z$ (MHz) | Comments   |
|---|-------|-------------|--|
| <b>No NaCl</b>                            |       |             |  |
| <i>LsAA9A</i> -H <sub>2</sub> O           | 2.279 | 458         | Weak superhyperfine (SHF) coupling   |
| <i>LsAA9A</i> +Cell <sub>6</sub>          | 2.273 | 515         | Intense SHF coupling   |
| <i>LsAA9A</i> +avicel                     | 2.278 | 470         | Weak SHF coupling  |
| <i>LsAA9A</i> +xylan                      | 2.272 | 480         | Spectrum complicated by organic-based radicals in perpendicular region   |
| <i>LsAA9A</i> +glucomannan                | 2.232 | 518         | Very likely NaCl contamination in the substrate. Intense SHF coupling  |
| <i>LsAA9A</i> +xyloglucan                 | 2.270 | 515         | Very intense SHF coupling.   |
| <b>200 mM NaCl</b>                        |       |             |  |
| <i>LsAA9A</i> -Cl                         | 2.258 | 455         | Likely mixture of H <sub>2</sub> O and Cl species.   |
| <i>LsAA9A</i> +Cell <sub>6</sub>          | 2.234 | 517         | Intense SHF coupling   |
| <i>LsAA9A</i> +avicel                     | 2.232 | 522         | Slight change in perpendicular region, some appearance of SHF coupling   |
| <i>LsAA9A</i> +xylan                      | 2.270 | 470         | Spectrum complicated by organic-based radicals in perpendicular region   |
| <i>LsAA9A</i> +solubilised xylan          | 2.272 | 470         | radical impurities present in the perpendicular region   |
| <i>LsAA9A</i> +glucomannan                | 2.231 | 520         | Intense SHF coupling   |
| <i>LsAA9A</i> +solubilised glucomannan    | 2.233 | 515         | Intense SHF coupling   |
| <i>LsAA9A</i> +xyloglucan                 | 2.228 | 530         | Intense SHF coupling   |
| <i>LsAA9A</i> +Xyl <sub>6</sub>           | 2.268 | 400         | Very rhombic, different from both Cell <sub>6</sub> -bound and unbound protein, intense SHF coupling. Could only be achieved with very high Xyl <sub>6</sub> concentrations. |
| <i>CvAA9A</i>                             | 2.273 | 476         | Likely no Cl species present   |
| <i>CvAA9A</i> +Cell <sub>6</sub>          | 2.228 | 527         | Mixture of C <sub>6</sub> -bound and unbound <i>CvAA9A</i> . Some SHF coupling visible. Full binding could not be achieved even with large excess of Cell <sub>6</sub>       |
| <i>CvAA9A</i> -1 M NaCl                   | 2.273 | 468         | Likely no Cl species present even in the presence of 1 M NaCl  |
| <i>CvAA9A</i> +Xyl <sub>6</sub> -1 M NaCl | 2.273 | 468         | Spectrum identical to the unbound form, even at very high Xyl <sub>6</sub> concentrations.   |

**Table 2: Spin-Hamiltonian parameters (parallel region) for *LsAA9A* and *CvAA9A* in contact with substrates.** The experiments were performed with or without 0.2 M chloride. For xylohexaose 1.0 M chloride was used. Spectra are shown in Supplementary Fig. 12–13.